Synthetic, physical and computational chemistry of propeller-shaped polycyclic aromatic hydrocarbons

Ham, A. van der

Chapter 4

Understanding the Conformational Preference of Propeller-shaped Polycyclic Aromatic Hydrocarbons

Abstract

In the previous Chapter the conformational preference of tripyrenylene was discussed in depth. A thermodynamic preference for a D_3 conformer was found, even though its synthesis was found to proceed under kinetic control to yield a C_2 product. This preference for a D_3 conformation is, however, not universal for all propellerenes, and the conformational behavior of propellerenes, in general, has been a standing question in the field. Because the physicochemical and photo-optical properties of propellerenes are highly dependent on their conformation, understanding the origin of the conformational preference of propellerenes is of paramount importance, if one wishes to rationally design propellerenes with specific physicochemical properties.

Parts of this Chapter are published as:

- van der Ham A., Hansen T., Overkleeft H. S., Filippov D. V., Hamlin T. A., Schneider G. F. Understanding the Conformational Preference of Propeller-shaped Polycyclic Aromatic Hydrocarbons. **Manuscript submitted.**
- van der Ham, A., Schneider, G. F., Lutz, Martin. CCDC 2056845: Experimental Crystal Structure Determination. **2021**, DOI: 10.5517/ccdc.csd.cc2719vg

Arguably the first propellerene to be synthesized was perfluorotriphenylene, whose crystal structure unequivocally showed it to reside in a counterintuitive C_2 symmetrical conformation.[1] Some 27 years later, Pascal *et al.* would successfully synthesize the elusive perchlorotriphenylene,[2,3] by the *in vacuo* pyrolysis of perchlorophthalic anhydride.[4] Crystallographically it, too, was found to reside in a highly twisted C_2 conformation. One year later the same group published a paper addressing this conformational conundrum for the first time.[5] Using semi-empirical and Hartree-Fock based computations they found that in the C_2 conformation the central ring of propellerenes adopts a puckered twist-boat configuration, whereas in the D_3 conformation the central ring adopts a more planar, chair-like configuration (Fig. 4.1). Conversely they observed the wings to be more planar in the C_2 conformation versus the D_3 conformation.[6] Based on these observations, in this initial report, they therefore concluded that the minimization of distortion from planarity of the wings in the C_2 conformation, at the expense of that of the central ring, was the key driving factor as to why a propellerene molecule would preferentially adopt a C_2 conformation.[6] This is additionally based on the notion that the wings and central ring are expected to behave as aromatic systems, *i.e.* distortion from planarity is resisted by the disruption of the π-conjugated system this would entail.

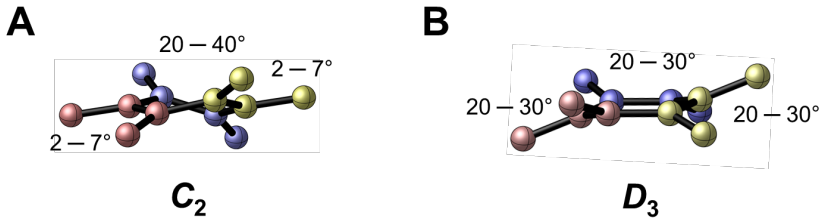

Figure 4.1 Representative geometries of the core fragment and radial bonds in the C_2 and D_3 conformation with key dihedral angles color-coded (pink, blue, yellow), with the range of angles found in **1-8**. This also illustrates the different ways in which the wings are adjoined to the core in the different conformations.

Although this theory seems to hold when considering only *ortho*-substituted triphenylenes, including *e.g.* hexamethyltriphenylene[7,8] and hexaiodotriphenylene,[9] it fails when π–extended, or benzoid, triphenylenes are considered, which all prefer a D_3 conformation. Realizing this problem, Pascal *et al.* published another, largely computational study in 1999, where they meticulously studied the geometry of a range of propellerenes in their different conformations.[10] There they argued that „*the C_2/D_3 dichotomy is a purely electronic effect*", as opposed to a steric one. Using a number of real and hypothetical molecules they stated the ability of bond alternation in the central ring to be key, asserting that „*The central ring geometry is not a product of the conformation, but a determining factor*". They additionally proposed a rule-of-thumb which states that when the circumference of the central ring is smaller than 8.5 Å a D_3 symmetry is preferred, whereas a C_2 symmetry is preferred when the circumference is larger than 8.6 Å. Interestingly, they proposed a molecule, colloquially known as „Pascal's super propellerene", which would invalidate this rule (See Chapter 6).

Many others have since tackled the question on the conformational behavior of propellerenes, both from a computational and experimental point of view, concluding a combination of aromatic, steric, and electrostatic factors to be at play in driving the conformational preference of propellerenes.[5,10-14] Recent advances in computational chemistry and expansion of the propellerene library prompted a revisit of this topic. Based on newly gained insights regarding the conformational behavior of propellerenes, it was hypothesized that the origin of the conformational preference of propellerenes could be rationalized from a balance in the individual preference of the central ring of the propellerene molecule and the wings attached thereto. To this end, a combined experimental and computational study was undertaken to elucidate and comprehensively describe the thermodynamic and kinetic factors that drive the conformational preference of propellerene molecules.

Model set and method validation. Notwithstanding the wide range of propellerenes known, to make the present study manageable, this Chapter focusses on a select set of triphenylene class of propellerenes (**1** – **8**), which constitutes the most studied class. Before continuing, it is important to define the two integral parts of propellerenes: the six central carbon atoms, called the *core*, and the rings and substituents attached thereto, collectively called the *wings* (highlighted in red and green, respectively, in Figure 4.2). Propellerenes can be further divided into two families based on the composition of the wings: those with substituents only on the *ortho*-position are denoted *ortho*-substituted (Fig. 4.2; **1** – **4**), whereas those with additional fused benzene rings are denoted as benzoid (Fig. 4.2; **5** – **8**), whereas those bearing. Experimentally, benzoid triphenylenes are reported to prefer a D_3 conformation, whereas *ortho*-substituted triphenylenes always prefer a C_2 conformation.

The geometries of this select set of triphenylene class propellerenes (**1** – **8**) were optimized at PBE-D3(BJ)/6-31G(d,p) in their C_2 and D_3 conformation (Fig. 4.2). Computed free Gibbs energies for the different conformers are in agreement with observed experimental preference of the propellerenes, both in gas phase (Fig. 4.2) and solution phase (Table S4.1), with all *ortho*-substituted triphenylenes (**1** – **4**) preferring a C_2 conformation,[8,9,12,15-18] and all benzoid triphenylenes (**5** – **8**) preferring a D_3 conformation (Fig. 4.2).[19-23] The ability of propellereness to interconvert between their two conformations at room temperature in solution was investigated. Computing of the corresponding transitions states gratifyingly gave values in good agreement with experimental values (Table S4.1). In short, with the exception of **1**, the barrier height to interconversion for all propellerenes, relative to the C_2 conformer (see Eq. 3), is sufficiently high ($\Delta G^{\ddagger}$ > 24 kcal mol^{-1}) to prevent spontaneous isomerization at room temperature (Table S4.1).

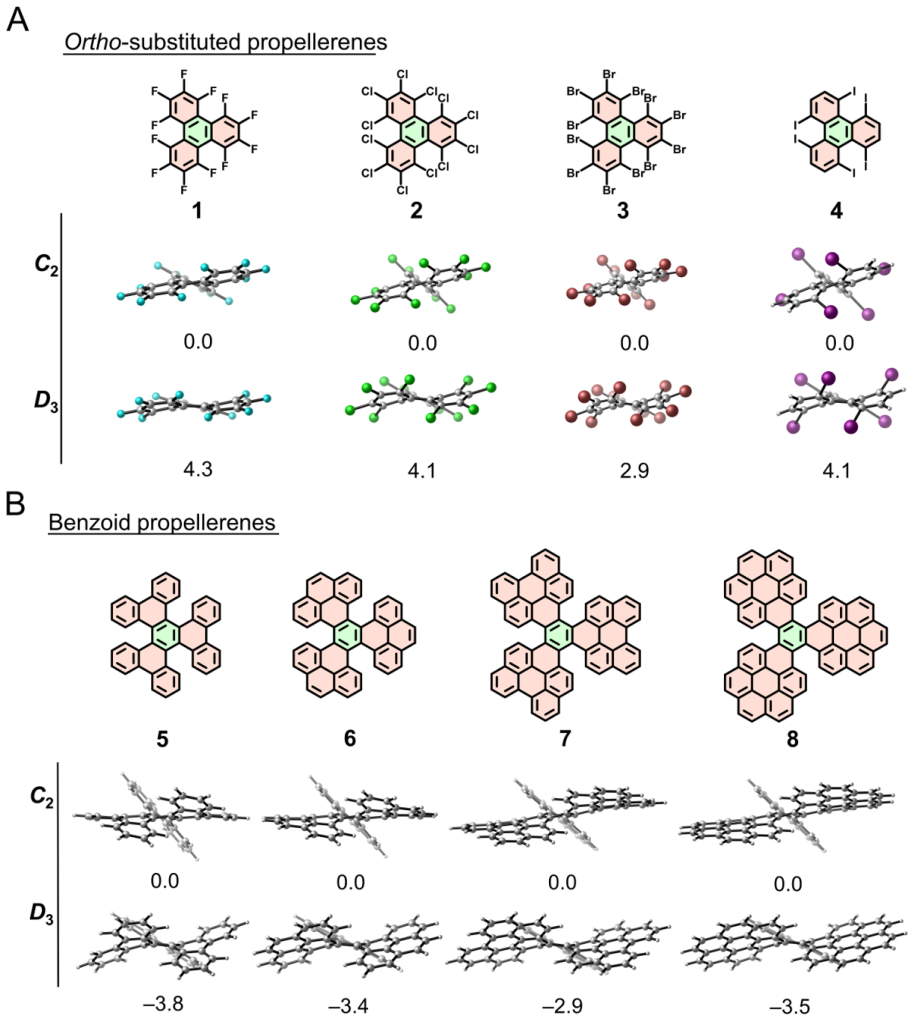

Figure 4.2 Structures and computed geometries of propellerenes **1-8** in the C_2 and D_3 conformation. The propellerenes have been grouped into the benzoid family (**1-4**; A) and the *ortho*-substituted family (**5-8**; B). The central rings have all been colored green and all wings have been colored red. Values provided below the structures are the Gibbs free energies (ΔG; kcal mol^{-1}) computed at PBE-D3(BJ)/6-31G(d,p), expressed relative to the energy of the C_2 conformer. For computational details see the Experimental.

Activation Strain Model. Having validated the computational method and having mapped the thermodynamic preference of the different propellerenes subclasses, attention is now directed at finding the origins of this preference. It was hypothesized that the balance between the intrinsic preferences of the core and the wings of a propellerene determines its most favorable conformation. To test this hypothesis, the activation strain model (ASM) was employed.[24] This computational model considers the rigidity of defined molecular fragments in a chemical system, as well as the ability of these fragments to interact with one another. Thus, in this model, the total energy of a system (ΔE_{tot}) is decomposed into a total strain term of all the molecular fragments (ΔE_{strain}), and an interaction energy term (ΔE_{int}):

$$\Delta E_{tot} = \Delta E_{strain} + \Delta E_{int} \qquad \text{(Eq. 1)}$$

Here, the strain energy, ΔE_{strain}, encompasses the penalty that needs to be paid in order to deform the molecular fragments from an initial state (here the C_2 conformation) to another state (here the D_3 conformation). The interaction energy term, ΔE_{int}, accounts for all the interactions that occur between these two molecular fragments in their different states (including both covalent and non-covalent interactions).

In the original ASM model, the different states of the molecular fragments are projected unto a reaction coordinate, typically describing bimolecular reactions,[25,26] (examples of dyotropic and cyclization reactions of unimolecular systems are also known in the literature).[27,28] However, for the present study, the ASM has to be extended to allow tracking of the changes in the ΔE_{strain} and ΔE_{int} terms experienced by *different parts of the same molecule*, in their two distinct conformations (Scheme 4.1). Therefore, to apply the ASM method in an insightful manner, the core and wings as defined above are designated as separate fragments. These are then cleaved homolytically to yield (uncharged) fragments with spins of +6 and –6 on the core and wings, respectively (Scheme 2). The analysis is then performed on the spin-restricted fragments in their spin-unrestricted electronic configuration. This approach is similar to that used by Krenske *et al.*[29-31] and others,[32] but differs in that in the present model, radicals are not capped and fragment geometries are not relaxed.

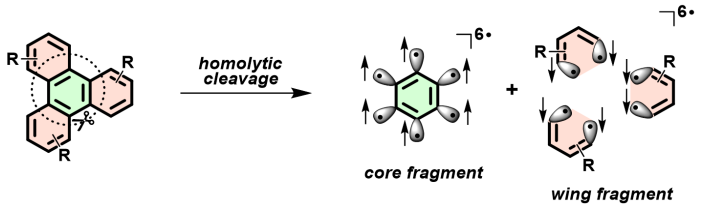

Scheme 4.1 Schematic representation of the homolytic cleavage of propellerenes to yield hexaradical core and wing fragments.

In the present model, the total energy of the propellerene system is further expressed as the sum of the strain experienced by the core ($\Delta E_{\text{strain}}^{\text{core}}$) and the wings fragments ($\Delta E_{\text{strain}}^{\text{wing}}$), and the interaction between them (ΔE_{int}; here primarily existing in the form of covalent C─C bonds). Equation 1 can thus be re-written as:

$$\Delta E_{\text{tot}} = \left(\Delta E_{\text{strain}}^{\text{core}} + \Delta E_{\text{strain}}^{\text{wing}}\right) + \Delta E_{\text{int}} \qquad \text{(Eq. 2)}$$

In the present study, all the energy terms are expressed with respect to the C_2 conformation (Eq. 3). As such, positive values of $\Delta\Delta E$ (as well as $\Delta\Delta G$ and $\Delta\Delta V$) indicate a preference for the C_2 conformation, whereas negative values represent a preference for the D_3 conformation.

$$\Delta\Delta E = \Delta E_{\text{tot}}^{D_3} - \Delta E_{\text{tot}}^{C_2} \qquad \text{(Eq. 3)}$$

Table 4.1 summarizes the results of the activation strain analysis (ASA). A sharp contrast is found between the total strain ($\Delta E_{\text{strain}}^{\text{total}}$), which is always more stabilizing in the C_2 conformation (with exception of entry **1** discussed later), and the interaction energy term (ΔE_{int}) which is always less destabilizing in the C_2 conformation. Decomposition of the total strain energy terms into the strain energies of the individual fragments (Eq. 2), reveals the core to always be less destabilizing in the C_2 conformation, whereas the wings are generally more destabilizing in this conformation. Exception to this is, again, perfluorotriphenylene **1**, whose wing strain shows a minor preference for the D_3 conformation.

Before further explaining these observations, it is important to reiterate that the wings in a propellerene molecule can only adopt two, geometrically possible arrangements, resulting in either a C_2 or D_3 symmetry of the propellerene molecule. The core, which is formed from the joining together of these wings, is therefore forced to adopt either a twist-boat or chair-like geometry, respectively (see Fig. 4.1 and 4.2). In other words, *the arrangement of the wings dictates the shape of the core*.

The wings. The aromatic wings of propellerenes have an intrinsic preference to be flat, yet their merger into a single molecule forces them to geometrically concede. Indeed, as highlighted in Figure 4.3, in the D_3 conformation, the wings are by and large planar, and thus unstrained, whereas steric congestion of the wings in the C_2 conformation necessitates a significant distortion from planarity. This desire of the wings to be flat is quantitatively reflected in their general preference for a D_3 conformation (Table 4.2). For the *ortho*-substituted propellerenes (**1** – **4**) a trend in $\Delta E_{\text{strain}}^{\text{wing}}$ is additionally found whereby an increase in the size of the substituents gives rise to an increase in destabilizing wing strain as F < Cl < Br < I, whereas for benzoid propellerenes no clear trend is observed. Propellerene **1** does not follow the general observation that the wings of propellerenes prefer a D_3 conformation of the molecule. It is observed that in **1** the rings directly attached to the propellerene core are more planar in the C_2 conformation than in the D_3 conformation, whereas the

Table 4.1 Activation strain and energy decomposition analysis of propellerenes **1-8**. All energies (kcal mol^{-1}) are computed at ZORA-PBE-D3(BJ)/TZ2P//PBE-D3(BJ)/6-31G(d,p) and are reported with respect to the C_2 conformation.

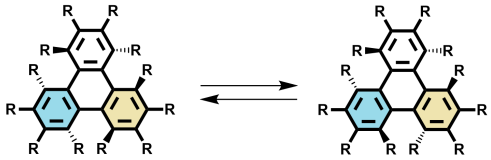

	$\Delta\Delta E$	$\Delta\Delta E^{\text{total}}_{\text{strain}}$	$\Delta\Delta E^{\text{core}}_{\text{strain}}$	$\Delta\Delta E^{\text{wing}}_{\text{strain}}$	$\Delta\Delta E_{\text{int}}$	$\Delta\Delta E_{\text{Pauli}}$	$\Delta\Delta V_{\text{elstat}}$	$\Delta\Delta E_{\text{oi}}$
1	5.0	1.2	0.9	0.4	3.8	–53.5	21.7	35.5
2	4.3	–2.3	1.9	–4.2	6.5	–74.9	34.3	47.1
3	3.1	–3.1	2.5	–5.6	6.3	–58.0	30.1	34.0
4	4.2	–3.2	3.3	–6.4	7.3	–135.6	45.0	97.8
5	–3.9	–6.9	1.5	–8.4	3.0	–52.2	22.8	32.4
6	–3.1	–5.0	1.3	–6.3	1.9	–48.2	19.5	30.6
7	–2.9	–4.8	2.1	–6.9	1.9	–49.6	18.6	32.8
8	–3.4	–5.1	1.0	–6.1	1.7	–59.8	21.8	39.7

substituents attached thereto (*i.e.* F) are bend more out-of-plane, than they are in the D_3 conformer. The balance between these two factors results in a preference for the C_2 conformation. It is important to note that *this balancing game is only possible for ortho-substituted wings, due to the relative flexibility of the unitary benzene ring, whereas benzoid extended wings are too rigid, and these will therefore always show a D_3 preference.*

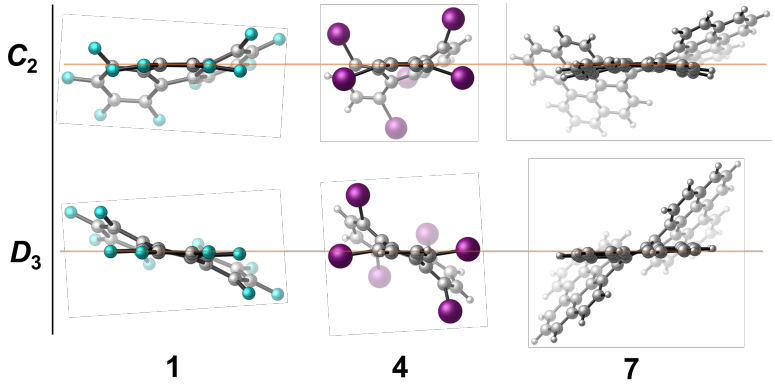

Figure 4.3 Side-view of propellerene **1**, **4** and **7**. Brown lines highlight the different extents of deformation (*i.e.* out-of-plane bending of the wings) in the C_2 conformation, compared to their relative planarity in the D_3 conformation.

The radial bonds. Within the ASM, the interaction energy term (ΔE_{int}) describes the interaction between two defined molecular fragments. In the present propellerene model, this constitutes the interaction between the core and wing fragments, and thus primarily concerns the covalent C─C bonds connecting the two fragments together. To better understand the interaction energy term, it can be decomposed into physically meaningful energy terms using a canonical energy decomposition analysis (EDA), to allow its analysis within the Kohn-Sham molecular orbital theory (KS-MO).[33-35] The EDA decomposes the ΔE_{int} into the following four physically meaningful energy terms:

$$\Delta E_{int} = \Delta V_{elstat} + \Delta E_{Pauli} + \Delta E_{oi} + \Delta E_{disp} \quad \text{(Eq. 4)}$$

Herein, ΔV_{elstat} is the electrostatic interaction between the unperturbed charge distributions of the (deformed) reactants and is usually attractive, ΔE_{Pauli} encompasses the destabilizing the Pauli repulsion between occupied closed-shell orbitals of both fragment, ΔE_{oi}, accounts for orbital interactions in the form of polarization and charge transfer between the fragments (*i.e.* HOMO–LUMO interactions) and ΔE_{disp} represents classical dispersion interactions between the fragments.

Looking at the radial bonds which connect the propellerene wings to the core, it is observed that they are shorter in the C_2 conformation than in the D_3 conformation, on the order of 0.01 Å. To verify whether observed trends in interaction energy between the wings and core (Table 4.1) originate from bond lengths alone, or whether the geometry of the bond attachment is of also importance, consistent geometry computations were performed. The radial bonds of propellerenes in their D_3 conformer were thus artificially shortened to be of the same length as in their corresponding C_2 conformer. This expectedly gave more stabilizing interaction energy as a result of more stabilizing ΔV_{elstat} and ΔE_{oi} terms, despite also giving more destabilizing ΔE_{Pauli}. Importantly, although absolute differences in ΔE_{int} between the two conformations became smaller, identical trends were still observed, indicating that the trends in ΔE_{int} (Table 4.1) are dictated by the way in which the radial bonds are attached, rather than by their lengths. Namely, in the C_2 conformation, the twist-boat geometry of the core allows two of the wings to join in an almost coplanar fashion, whereas in the D_3 conformation the chair-like geometry of the ring dictates a more skewed attachment of the wings (Fig. 4.1; highlighted pink and yellow). As a result, the orbital overlap is less favorable in the more skewed D_3 conformation, compared to the C_2 conformation.

It was additionally noted that, as the radial bonds were shortened to that of the C_2 conformer, the total strain of the propellerenes became more destabilizing, located solely on the wings. This is due to the fact that, as the radial bonds are shortened, the wings approach each other at closer distances, and despite the differences in radial bond length being only minute, an increase in destabilizing strain of up to 19.5 kcal mol^{-1} was found in the case of 6. When radial bonds in C_2 conformers were artificially lengthened, an opposite effect was found.

The core. Conversely with the radial bonds, the C—C bonds within the core of propellerenes are always longer in the C_2 conformation than in the D_3 conformation; *i.e.* the core of the C_2 conformer is larger than that of the D_3 conformer. To understand whether the preference of the core for a C_2 conformation is due to these differences in bond length or whether it stems from an intrinsic preference for the geometry of a twist-boat conformation, a numerical experiment was performed. Bond lengths of propellerene core fragments in their C_2 and D_3 conformation were constrained and all dihedral angles were artificially set to 0°, forcing the rings to become flat. Surprisingly, absolute differences in total energy diminished, and even shifted in favor of the D_3 conformation (Table 4.2). As an exemplary experiment, when the bare core was allowed to relax further, without constrains, bond lengths became even shorter and a planar, benzene-like molecule was obtained. Thus, the core of a propellerene molecule ideally wants to have shorter C—C bonds, however, in the context of a propellerene is geometrically prohibited from doing so by the presence of the wings. These findings reinforce the notion that that the conformation of the core is enforced by the wings, rather than the other way around, and corrects the previous assertion of Pascal *et al.* that "*the core geometry is not a product of the conformation*".[10,36-41]

Table 4.2 Numerical experiments on the core fragments of propellerenes **1-8**. $\Delta\Delta E_{int}$ denotes the difference in single point energy of the core after planarization with fixed bond lengths, compared to that computed in their original C_2 and D_3 conformation. All energies computed at ZORA-PBE-D3(BJ)/TZ2P//PBE-D3(BJ)/6-31G(d,p) (kcal mol^{-1}), reported with respect to the $C_2 \rightarrow D_3$ conversion.

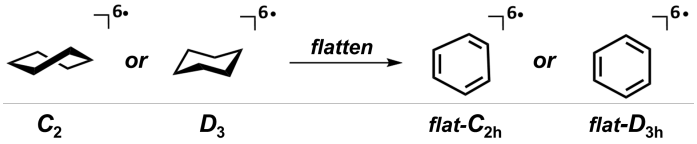

	$\Delta\Delta E_{int}$
1	–0.9
2	–1.3
3	–3.6
4	–1.5
5	–0.3
6	–0.3
7	–0.8
8	–4.9

Combining the ASM and EDA analyses, it can be concluded that propellerenes have two choices: (i) either have shorter radial bonds between the wings and the core, resulting in more stabilizing interaction energy between the wings and core, however also more congested wings (more destabilizing steric repulsion between the wings), or (ii) have longer radial bonds, giving rise to less stabilizing ΔE_{int}, while also giving less congested wings (less destabilizing steric repulsion between the wings). In other words, the balance at play is not so much between the core and the wings, but between the wings and the bonds connecting them to the core. Furthermore, when wings of the propellerene are rigid (*i.e.* benzoid triphenylenes), a D_3 conformation will always be preferred, as this conformation minimizes steric repulsion between the wings, which is able to overcome the intrinsic C_2 preference of the core and radial bonds. In contrast, the relative flexibility of *ortho*-substituted wings results in a lesser degree of D_3 preference or even a C_2 preference, and which allows the core and radial bonds to dictate the adaptation of a C_2 conformation. It is this dichotomy that uniquely sets benzoid propellerenes apart from the ortho-substituted family. This interplay is graphically illustrated in Figure S4.3.

Model validation. To validate this hypothesis, additional molecules (**9** – **11**) were selected and analysed using the present model (Table 4.3). These molecules all have alkyl substituents on the *ortho* position. It is observed that compound 9 follows the general trend observed for the halogenated propellerenes (Table 4.2), i.e. the wings prefer a D_3 conformation, whereas the core and radial bonds prefer a C_2 conformation, the latter term of which is able to overcompensate the total strain term. Compounds **9** and **11**, however behave more like perfluorotriphenylene **1** in which all terms, including the wings, prefer a C_2 conformation. This is accounted for by the present model, as the preference of *ortho* substituted propellerenes for a C_2 conformation is related to the ability of the substituents to bend. Compound **11** is a particularly interesting case, being the hydrogenated variant of **2**, which prefers a D_3 conformation. In other words, upon hydrogenation of **2**, the *ortho*-carbons of the wings change from sp^2 to sp^3, making them more flexible, causing a shift in preference from D_3 to C_2. To further illustrate this point, the structure of an extreme example, hexa-adamantyltriphenylene **12** was also computed (Figure S4.4). It was found that, despite belonging to the *ortho*-substituted family of propellerenes, **12** still prefers a D_3 conformation. This is because the extreme steric bulk of the adamantyl moieties prevents them from bending out-of-plane.

Table 4.2 Activation strain and energy decomposition analysis of propellerenes **9** – **11**. All energies (kcal mol^{-1}) are computed at ZORA-PBE-D3(BJ)/TZ2P//PBE-D3(BJ)/6-31G(d,p) and are reported with respect to the C_2 conformation.

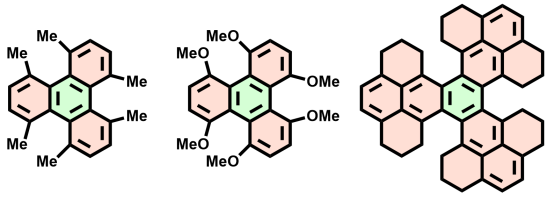

9 **10** **11**

	$\Delta\Delta E$	$\Delta\Delta E^{\text{total}}_{\text{strain}}$	$\Delta\Delta E^{\text{core}}_{\text{strain}}$	$\Delta\Delta E^{\text{wing}}_{\text{strain}}$	$\Delta\Delta E_{\text{int}}$	$\Delta\Delta E_{\text{Pauli}}$	$\Delta\Delta V_{\text{elstat}}$	$\Delta\Delta E_{\text{oi}}$
9	4.9	3.3	3.3	0.0	1.6	–133.3	52.6	88.2
10	3.3	–4.3	2.7	–7.0	7.6	168.2	–35.4	–125.0
11	4.2	2.8	2.4	0.4	1.4	61.9	–22.0	–38.9

Combined, based on the ASA, it is found that the integral propellerene parts all share the same characteristics in both propellerene families. Importantly, it is the magnitude of the interaction energy between the core and the wings that varies most between the two families, and ultimately lays at the heart of the sharp contrast in conformational preference between *ortho*- and benzoid-substituted propellerenes. The magnitude of the interaction energy is, in turn, dictated by the flexibility of the propellerene wings. When wings are relatively flexible (*i.e*. *ortho*-substituted propellerenes) they are able to adopt a more distorted C_2 conformation, allowing for shorter radial bonds between the core and the wings, with concomitantly more a stabilizing interaction energy. In contrast, more rigid wings cannot deform sufficiently (*i.e*. benzoid-substituted propellerenes), and thus necessitate longer radial bonds to avoid steric clash between the wings, and incurring less stabilizing interaction energy (Fig. 4.4). This interplay between the flexibility of the wings and length of the radial bonds is graphically illustrated in Figure 4.5. There it is apparent that for *ortho*-substituted propellerenes, conversion from the C_2 conformation to the D_3 conformation is associated with flatter wings (favorable) but also longer radial bonds (unfavorable), whereas for the benzoid-substituted propellerenes there is hardly any change in radial bond length during interconversion, and the preference for a D_3 conformation is thus purely dictated by the relative planarity of the wings in the two conformations.

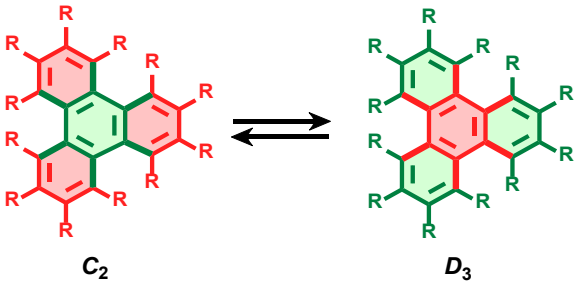

Figure 4.4. Schematic overview of the $C_2 \rightleftarrows D_3$ interconversion of propellerenes to graphically illustrate that the wings of propellerenes prefer to adopt the D_3 conformation, whereas the radial bonds and core want to reside in a more distorted C_2 conformation. The green color indicates that the fragment prefers the specific conformation, while the opposite is true for the red color. Radial bonds drawn in bold.

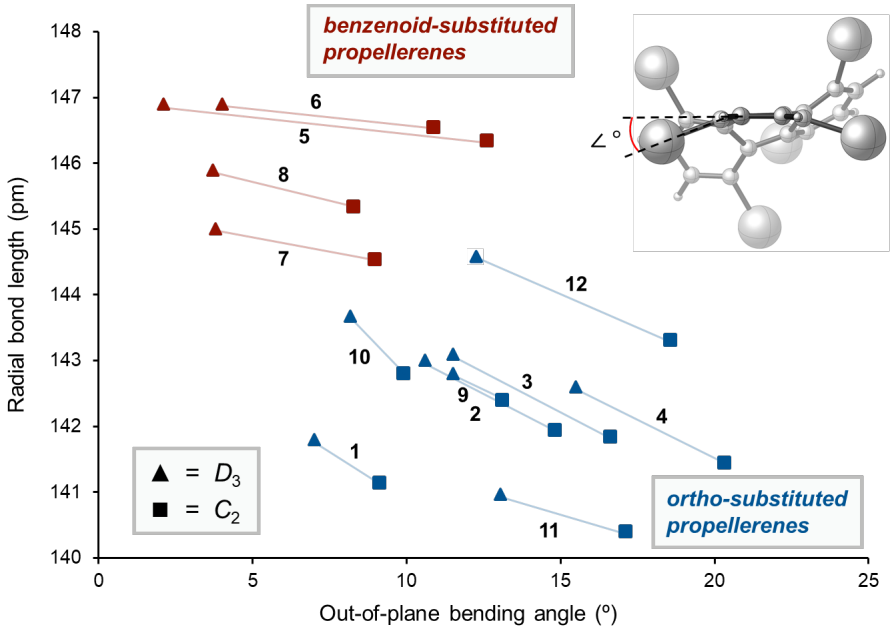

Figure 4.5. Plot of the average radial bond length as a function of the average bending angle of wings of propellerenes **1**-**8** in the C_2 and D_3 conformation. Compounds and conformations are groups as: benzoid-C_2 (brown squares), benzoid-D_3 (brown triangles), *ortho*-C_2 (blue squares) and *ortho*-D_3 (blue triangles). The definition of the out-of-plane bending angle is illustrated in the top right corner.

To conclude, the conformational preference of propeller-shaped polycyclic aromatic hydrocarbons has been the topic of heavy debate. Triphenylene-class propellerenes with substituents on the *ortho*-position prefer to adopt a conformation with a C_2 conformation, whereas those with benzoid substituents prefer to adopt a D_3 conformation. Herein, a comprehensible framework is provided that rationalizes the driving forces behind the conformational preference of a range of structurally diverse propellerenes.

The origin of the thermodynamic preference of propellerenes could be quantified using a novel adaptation of the activation strain model (ASM). By strategically fragmenting propellerene molecules, it is found that both the core and wings of propellerenes desire to be flat, however, their merger necessitates significant deformation, away from their ideal geometry, to minimize steric interactions between the wings. The desire of the wings for the D_3 conformation to always be greater than the desire of the core for a C_2 conformation. Attention is therefore shifted to the radial bonds, which connect the core and wings together. These were also found to always prefer a C_2 conformation and, in the case of *ortho*-substituted propellerenes, are even able to overrule the preference of the wings. It was ultimately concluded that the balance at play in propellerenes is between *the extent to which the wings can bend and the radial bonds can contract*. When wings are flexible, a C_2 conformation will be preferred, when wings are rigid, a D_3 conformation will always be preferred.

These findings will equip experimentalists with the insight to understand and rationalize the trends in conformational behavior of propellerenes and allow the tailor-made design of novel sterically congested structures. Although applied here only to propellerenes, the present methodology is broadly applicable and will open up new avenues not only in the field of PAH research but in the field of physical chemistry at large, and should prove useful in the rational design of novel functional constructs.

References

(1) Hursthouse, M. B.; Smith, V. B.; Massey, A. G. The crystal and molecular structure of dodecafluorotriphenylene, C18F12. *J. Fluor. Chem.* **1977,** *10* (2), 145.

(2) Campbell, M. C.; Humphries, R. E.; Munn, N. M. Perchlorotriphenylene: a compound with severe molecular twisting? *J. Org. Chem.* **1992,** *57* (2), 641.

(3) Gall, J. H.; MacNicol, D. D.; Mallinson, P. R.; Welsh, P. A. Discovery and crystal structure of a novel chlorocarbon host: perchlorofluorene-9-spirocyclohexa-2′,5′-diene. *Tet. Lett.* **1985,** *26* (33), 4005.

(4) Shibata, K.; Kulkarni, A. A.; Ho, D. M.; Pascal Jr, R. A. Perchlorotriphenylene. *J. Am. Chem. Soc.* **1994,** *116* (13), 5983.

(5) Shibata, K.; Kulkarni, A. A.; Ho, D. M.; Pascal Jr, R. A. The Pursuit of Perchlorotriphenylene. *J. Org. Chem.* **1995,** *60* (2), 428.

(6) In their study, Pascal *et al.* considered only the carbon framework when commenting on the relative planarity of the wings. In the present study, the out-of-plane bending of the ortho substituents is also included.

(7) Chen, L.; Zhang, C.; Wen, C.; Zhang, K.; Liu, W.; Chen, Q. Gold-catalyzed cyclotrimerization of arynes for the synthesis of triphenylenes. *Catal. Commun.* **2015,** *65*, 81.

(8) Wang, Y.; Stretton, A. D.; McConnell, M. C.; Wood, P. A.; Parsons, S.; Henry, J. B.; Mount, A. R.; Galow, T. H. 1,4,5,8,9,12-hexamethyltriphenylene. A molecule with a flipping twist. *J. Am. Chem. Soc.* **2007,** *129* (43), 13193.

(9) Tan, Q.; Zhou, D.; Zhang, T.; Liu, B.; Xu, B. Iodine-doped sumanene and its application for the synthesis of chalcogenasumanenes and silasumanenes. *Chem. Comm.* **2017,** *53* (74), 10279.

(10) Barnett, L.; Ho, D. M.; Baldridge, K. K.; Pascal, R. A. The Structure of Hexabenzotriphenylene and the Problem of Overcrowded "D3h" Polycyclic Aromatic Compounds. *J. Am. Chem. Soc.* **1999,** *121* (4), 727.

(11) Balaban, A. T.; Randić, M. *Structural approach to aromaticity and local aromaticity in conjugated polycyclic systems*; Springer, 2011.

(12) Smith, V. B.; Massey, A. G. Perfluorophenyl derivatives of the elements—XXII: Perfluorotriphenylene. *Tetrahedron* **1969,** *25* (22), 5495.

(13) Coe, P. L.; Stephens, R.; Tatlow, J. C. 622. Aromatic polyfluoro-compounds. Part XI. Pentafluoro-phenyl-lithium and derived compounds. *J. Chem. Soc. (Resumed)* **1962**, 3227.

(14) Falk, R. A. Hexafluorobenzene and related fluoroaromatic compounds (Thermal and radiation stability of aromatic fluorocarbons makes them useful as plastics, lubricants, hydraulic and gyroscopic fluids and heat transfer fluids for nuclear powerplants). *Sperry Eng. Rev.* **1963,** *16*, 24.

(15) Naritomi, M.; Murofushi, H.; Nakashima, N. Dopants for a perfluorinated graded index polymer optical fiber. *Bull. Chem. Soc. Jap.* **2004,** *77* (11), 2121.

(16) Frampton, C. S.; MacNicol, D. D.; Rowan, S. J. Synthesis and structural properties of the first dodecakis (aryloxy) triphenylenes. *J. Mol. Struct.* **1997,** *405* (2-3), 169.

(17) Nishinaga, T.; Inoue, R.; Matsuura, A.; Komatsu, K. Formation of a novel arenium ion from the radical cation of a twisted triphenylene fully annelated with bicyclo [2.2. 2] octene units. *Org. Lett.* **2002,** *4* (9), 1435.

(18) Li, Z.; Zhi, L.; Lucas, N. T.; Wang, Z. Triangle-shaped polycyclic aromatics based on tribenzocoronene: facile synthesis and physical properties. *Tetrahedron* **2009,** *65* (17), 3417.

(19) Hosokawa, T.; Takahashi, Y.; Matsushima, T.; Watanabe, S.; Kikkawa, S.; Azumaya, I.; Tsurusaki, A.; Kamikawa, K. Synthesis, structures, and properties of hexapole helicenes: Assembling six [5]helicene substructures into highly twisted aromatic systems. *J. Am. Chem. Soc.* **2017,** *139* (51), 18512.

(20) Berezhnaia, V.; Roy, M.; Vanthuyne, N.; Villa, M.; Naubron, J.-V. r.; Rodriguez, J.; Coquerel, Y.; Gingras, M. Chiral nanographene propeller embedding six enantiomerically stable [5]helicene units. *J. Am. Chem. Soc.* **2017,** *139* (51), 18508.

(21) Zuzak, R.; Castro-Esteban, J.; Brandimarte, P.; Engelund, M.; Cobas, A.; Piątkowski, P.; Kolmer, M.; Pérez, D.; Guitián, E.; Szymonski, M. Building a 22-ring nanographene by combining in-solution and on-surface syntheses. *Chem. Comm.* **2018,** *54* (73), 10256.

(22) Peña, D.; Cobas, A.; Pérez, D.; Guitián, E.; Castedo, L. Kinetic control in the palladium-catalyzed synthesis of C_2-symmetric hexabenzotriphenylene. A conformational study. *Org. Lett.* **2000,** *2* (11), 1629.

(23) Pradhan, A.; Dechambenoit, P.; Bock, H.; Durola, F. Twisted polycyclic arenes by intramolecular Scholl reactions of C_3-symmetric precursors. *J. Org. Chem.* **2013,** *78* (6), 2266.

(24) For a step-by-step protocol, see: a) P. Vermeeren, S. C. C. van der Lubbe, C. Fonseca Guerra, F. M. Bickelhaupt, T. A. Hamlin, *Nat. Protoc.* **2020**, *15*, 649; for reviews, see: b) F. M. Bickelhaupt, *J. Comp. Chem.* **1999**, *20*, 114; c) W.-J. van Zeist, F. M. Bickelhaupt, *Org. Biomol. Chem.* **2010**, *8*, 3118; d) I. Fernández, F. M. Bickelhaupt, *Chem. Soc. Rev.* **2014**, *43*, 4953; e) L. P. Wolters, F. M. Bickelhaupt, *WIRES Comput. Mol. Sci.* **2015**, 5, 324; f) F. M. Bickelhaupt, K. N. Houk, *Angew. Chem.* **2017**, *129*, 10204; *Angew. Chem. Int. Ed.* **2017**, *56*, 10070.

(25) Vermeeren, P.; Hansen, T.; Grasser, M.; Silva, D. R.; Hamlin, T. A.; Bickelhaupt, F. M. SN2 versus E2 competition of F– and PH2– revisited. *J. Org. Chem.* **2020,** *85* (21), 14087.

(26) Vermeeren, P.; Hansen, T.; Jansen, P.; Swart, M.; Hamlin, T. A.; Bickelhaupt, F. M. A unified framework for understanding nucleophilicity and protophilicity in the SN2/E2 competition. *Chem.-Eur. J.* **2020,** *26* (67), 15538.

(27) Fernández, I.; Bickelhaupt, F. M.; Cossío, F. P. Ene-ene-yne reactions: Activation strain analysis and the role of aromaticity. *Chem. Eur. J.* **2014,** *20* (34), 10791.

(28) Fernández, I.; Bickelhaupt, F. M.; Cossío, F. P. Type-I dyotropic reactions: understanding trends in barriers. *Chem. Eur. J.* **2012,** *18* (39), 12395.

(29) Krenske, E. H.; Houk, K. N.; Holmes, A. B.; Thompson, J. Entropy versus tether strain effects on rates of intramolecular 1,3-dipolar cycloadditions of *N*-alkenylnitrones. *Tet. Lett.* **2011,** *52* (17), 2181.

(30) Krenske, E. H.; Davison, E. C.; Forbes, I. T.; Warner, J. A.; Smith, A. L.; Holmes, A. B.; Houk, K. N. Reverse cope elimination of hydroxylamines and alkenes or alkynes: theoretical investigation of tether length and substituent effects. *J. Am. Chem. Soc.* **2012,** *134* (4), 2434.

(31) Krenske, E. H.; Perry, E. W.; Jerome, S. V.; Maimone, T. J.; Baran, P. S.; Houk, K. N. Why a Proximity-Induced Diels–Alder Reaction is So Fast. *Org. Lett.* **2012,** *14* (12), 3016.

(32) Gold, B.; Shevchenko, N. E.; Bonus, N.; Dudley, G. B.; Alabugin, I. V. Selective transition state stabilization via hyperconjugative and conjugative assistance: stereoelectronic concept for copper-free click chemistry. *J. Org. Chem.* **2011,** *77* (1), 75.

(33) Bickelhaupt, F. M.; Baerends, E. J.; John Wiley and Sons New York, NY, USA, 2000; Vol. 15.

(34) Van Meer, R.; Gritsenko, O. V.; Baerends, E. J. Physical meaning of virtual Kohn–Sham orbitals and orbital energies: an ideal basis for the description of molecular excitations. *J. Chem. Theo. Comp.* **2014,** *10* (10), 4432.

(35) a) Zhao, L.; von Hopffgarten, M.; Andrada, D. M. *WIRES Comput. Mol. Sci.* **2018**, *8*, e1345; b) G. Frenking, FM Bickelhaupt. *The EDA Perspective of Chemical Bonding in The Chemical Bond. Fundamental Aspects of Chemical Bonding* **2014,** *4*, 121.

(36) Although the exact reason for the preference of the core for a C_2 conformation could not be elucidated, these findings corroborate those made by others which found the central ring of propellerenes to be poorly or even non-aromatic; *i.e.* aromaticity and thus a drive to planarity are not significant factors in determining the conformational preference of the core in the context of a propellerene molecule. See the following references.

(37) Fernandez, I.; Frenking, G. Direct estimate of conjugation and aromaticity in cyclic compounds with the EDA method. *Faraday Discuss.* **2007,** *135*, 403.

(38) Pierrefixe, S. C. A. H.; Bickelhaupt, F. M. Aromaticity: molecular-orbital picture of an intuitive concept. *Chem. Eur. J.* **2007,** *13* (22), 6321.
(39) Roy, M.; Berezhnaia, V.; Villa, M.; Vanthuyne, N.; Giorgi, M.; Naubron, J. V.; Poyer, S.; Monnier, V.; Charles, L.; Carissan, Y. Stereoselective syntheses, structures, and properties of extremely distorted chiral nanographenes embedding hextuple helicenes. *Angew. Chem. Int. Ed.* **2020,** *59* (8), 3264.
(40) Antić, M.; Furtula, B.; Radenkovic, S. Aromaticity of nonplanar fully benzenoid hydrocarbons. *J. Phys. Chem. A* **2017,** *121* (18), 3616.
(41) Hosokawa, T.; Tsurusaki, A.; Kamikawa, K. Assembly of [5]helicene subunits by palladium-catalyzed reactions: Synthesis, structures, properties, and theoretical study of multiple helicenes. *J. Synth. Org. Chem. Jap.* **2020,** *78* (11), 1013.
(42) Chang, N.-h.; Chen, X.-c.; Nonobe, H.; Okuda, Y.; Mori, H.; Nakajima, K.; Nishihara, Y. Synthesis of substituted picenes through Pd-catalyzed cross-coupling reaction/annulation sequences and their physicochemical properties. *Org. Lett.* **2013,** *15* (14), 3558.
(43) Macrae, C. F.; Sovago, I.; Cottrell, S. J.; Galek, P. T. A.; McCabe, P.; Pidcock, E.; Platings, M.; Shields, G. P.; Stevens, J. S.; Towler, M. Mercury 4.0: From visualization to analysis, design and prediction. *J. Appl. Crystallogr.* **2020,** *53* (1), 226.
(44) Shao, Y.; Molnar, L. F.; Jung, Y.; Kussmann, J.; Ochsenfeld, C.; Brown, S. T.; Gilbert, A. T. B.; Slipchenko, L. V.; Levchenko, S. V.; O'Neill, D. P. Advances in methods and algorithms in a modern quantum chemistry program package. *Phys. Chem. Chem. Phys.* **2006,** *8* (27), 3172.
(45) Frisch, M. J.; Trucks, G. W.; Schlegel, H. B.; Scuseria, G. E.; Robb, M. A.; Cheeseman, J. R.; Scalmani, G.; Barone, V.; Mennucci, B.; Petersson, G. A. Gaussian 09 Revision D. 01, 2009. *Gaussian Inc. Wallingford CT* **2009**.
(46) PBE was used as both exchange and correlation functional, and was called using the pbepbe keyword in the Gaussian 09 software. At the DFT-D3(BJ) level of theory the s6 and s8 values are set to 1 and 0.7875 respectively, whereas the ABJ1 and ABJ2 values are set respectively to 0.4289 and 4.4407.
(47) Grimme, S.; Antony, J.; Ehrlich, S.; Krieg, H. A consistent and accurate ab initio parametrization of density functional dispersion correction (DFT-D) for the 94 elements H-Pu. *J. Chem. Phys.* **2010,** *132* (15), 154104.
(48) Grimme, S.; Ehrlich, S.; Goerigk, L. Effect of the damping function in dispersion corrected density functional theory. *J. Comp. Chem.* **2011,** *32* (7), 1456.
(49) Hay, P. J.; Wadt, W. R. Ab initio effective core potentials for molecular calculations. Potentials for K to Au including the outermost core orbitals. *J. Chem. Phys.* **1985,** *82* (1), 299.
(50) Karton, A. How reliable is DFT in predicting relative energies of polycyclic aromatic hydrocarbon isomers? comparison of functionals from different rungs of jacob's ladder. *J. Comp. Chem.* **2017,** *38* (6), 370.
(51) Minenkov, Y.; Singstad, Å.; Occhipinti, G.; Jensen, V. R. The accuracy of DFT-optimized geometries of functional transition metal compounds: a validation study of catalysts for olefin metathesis and other reactions in the homogeneous phase. *Dalton T.* **2012,** *41* (18), 5526.
(52) Sperger, T.; Fisher, H. C.; Schoenebeck, F. Computationally deciphering palladium-catalyzed reaction mechanisms. *WIRES Comp. Mol. Sci.* **2016,** *6* (3), 226.
(53) Josa, D.; Rodríguez-Otero, J.; Cabaleiro-Lago, E. M.; Rellán-Piñeiro, M. Analysis of the performance of DFT-D, M05-2X and M06-2X functionals for studying π···π interactions. *Chem. Phys. Lett.* **2013,** *557*, 170.
(54) Marenich, A. V.; Cramer, C. J.; Truhlar, D. G. Universal solvation model based on solute electron density and on a continuum model of the solvent defined by the bulk dielectric constant and atomic surface tensions. *J. Phys. Chem. B* **2009,** *113* (18), 6378.
(55) Bootsma, A. N.; Wheeler, S. E. Popular Integration Grids Can Result in Large Errors in DFT-Computed Free Energies. *ChemRxiv. Preprint* **2019**.

(56) Ribeiro, R. F.; Marenich, A. V.; Cramer, C. J.; Truhlar, D. G. Use of solution-phase vibrational frequencies in continuum models for the free energy of solvation. *J. Phys. Chem. B* **2011,** *115* (49), 14556.
(57) Funes-Ardoiz, I.; Paton, R. S. **2016**. GoodVibes: GoodVibes v1.0.2. http://doi.org/10.5281/zenodo.595246.
(58) Legault, C. Y. *CYLview, 1.0 b, Université de Sherbrooke, 2009*, 2013.
(59) ADF2017.103, SCM Theoretical Chemistry, Vrije Universiteit : Amsterdam (Netherlands), **2010**. http://www.scm.com.
(60) te Velde, G.; Bickelhaupt, F. M.; Baerends, E. J.; Fonseca Guerra, C.; Van Gisbergen, S. J. A.; Snijders, J. G.; Ziegler, T. Chemistry with ADF. *J. Comp. Chem.* **2001,** *22* (9), 931.
(61) Fonseca Guerra, C.; Snijders, J. G.; te Velde, G.; Baerends, E. J. Towards an order-N DFT method. *Theo. Chem. Acc.* **1998,** *99* (6), 391.
(62) Cosmo, R.; Sternhell, S. Steric effects. Inversion of 4,5-disubstituted 9,10-dihydrophenanthrenes. *Austr. J. Chem.* **1987,** *40* (1), 35.
(63) Cosmo, R.; Hambley, T. W.; Sternhell, S. Skeletal deformation in 4,5-disubstituted 9, 10-dihydrophenanthrenes and 4, 5-disubstituted phenanthrenes. *J. Org. Chem.* **1987,** *52* (14), 3119.
(64) Based on the absence of observable interconversion after 20 hrs at 70 °C.

Experimental

Synthesis. All reagents were obtained from commercial sources and were used as received. Solvents used were stored over 4 Å molecular sieves. Reactions were monitored by TLC analysis using Merck 25 DC plastikfolien 60 F254 with detection by using an aqueous solution of $KMnO_4$ (7%) and K_2CO_3 (2%) followed by charring at ~150 °C. Column chromatography was performed on Fluka silica gel (0.04–0.063 mm). High-resolution mass spectra were recorded by direct injection (2 µL of a 2 µM solution in water/acetonitrile; 50:50; v/v and 0.1% formic acid) on a mass spectrometer (Thermo Finnigan LTQ Orbitrap) equipped with an electrospray ion source in positive mode (source voltage 3.5 kV, sheath gas flow 10, capillary temperature 250 °C). The high-resolution mass spectrometer was calibrated prior to measurements with a calibration mixture (Thermo Finnigan). All NMR experiments were performed on a Bruker AV500 NMR instrument equipped with a BBFO probe head for 5 mm outer diameter tubes. Spectra were recorded at 500 MHz for ^{1}H, 125 MHz for ^{13}C and 470 MHz for ^{19}F. All deuterated solvents were obtained from a commercial source (Eurisotop) and were used as received. Chemical shifts are given in ppm (δ) relative to TMS (0 ppm), and coupling constants (*J*) are given in hertz (Hz). For synthetic procedures and NMR data related to HBT (**5**) and tripyrenylene (**6**) see the previous Chapter.

Perfluorotriphenylene (1)[12]

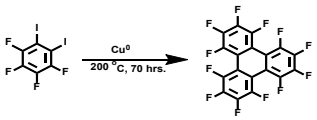

A crimp top vial, which had been flame dried under vacuum, was charged with an intimate mixture of 1,2-diiodotetrafluorobenzene (3 g, 2.5 mmol) and copper powder (3 g). The tube was sealed, evacuated to high vacuum (< 1 mbar) and then heated on a metal block to 200°C for 70 hrs. After cooling down to room temperature, the tube was backfilled with argon and opened. The sublimate of colorless to pale pink crystals was removed and identified as nearly pure perfluorotriphenylene (217 mg, 0.49 mmol, 19.6%). ^{13}C NMR (125 MHz, THF-d_8) δ 143.8 (dt, $^1J_{CF}$ = 260 Hz, $^3J_{CF}$ = 13 Hz), 140.9 (dd, $^1J_{CF}$ = 264 Hz, $^3J_{CF}$ = 11 Hz), 121.1 (br t, $^2J_{CF}$ = 9.5 Hz); ^{19}F NMR (471 MHz, THF-d_8) δ -141.7 (d, $^3J_{FF}$ = 13 Hz), -152.2 (d, $^3J_{FF}$ = 13 Hz). MALDI-TOF calc'd 444.1788 m/z, found 444.659 m/z.

1,4-Dichloro-2,3-diiodobenzene (13)[42]

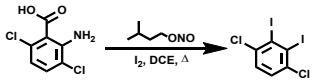

A solution of isoamyl nitrite (1.6 mL, 1.40 g, 6 mmol) and iodine (4.54 g, 5 mmol) in 1,2-dichloroethane (200 mL) was heated to reflux and a solution of 2,5-dichloroanthranilic acid (1.03 g, 2.5 mmol) in dioxane (25 mL) added over a period of 20 min. The mixture was refluxed for 1h, then cooled and filtered. The filtrate was washed with aqueous 5% $Na_2S_2O_4$ (2x 50ml), 1M HCl (1x 25 mL) and brine (1x 25 mL). The organic layer was dried over $MgSO_4$, filtered and evaporated to dryness. The residue was purified by column chromatography over silica gel using neat pentane as eluent to provide 1,4-dichloro-2,3-diiodobenzene as a white crystalline solid. Yield: 1.0 g, 2.5 mmol, quant. ^{1}H NMR (500MHz, $CDCl_3$) δ 7.42 (s, 2H). ^{13}C NMR (125MHZ, $CDCl_3$) δ 137.03, 129.28, 114.97.

1,4,5,8,9,12-Hexachlorotriphenylene (14) // 1,4,5,8-tetrachlorobiphenylene (15)

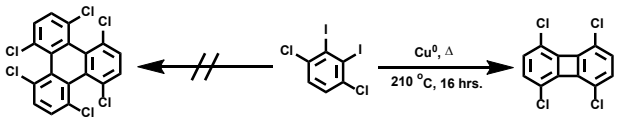

The 1,4-dichloro-2,3-diiodobenzene (0.5 g) was intimately mixed with copper powder (2 g) and charged in a shrink cap vial which had previously been flame dried under high vacuum and back-purged with dry argon gas. The vial was sealed, evacuated to high vacuum and heated on a heating block to 210°C for a total of 16 hrs. A pale yellow crystalline sublimate was careful removed from the upper part of the vial (Fig. S4.1A). ^{1}H NMR (850MHz, $CDCl_3$) δ 6.70 (s, 4H). ^{13}C NMR (212MHz, $CDCl_3$) δ 145.45, 132.20, 122.16. The remainder of material was dissolved in DCM, filtered twice over glass wool, and the resultant dark orange solution evaporated under reduced pressure. NMR spectroscopy indicated an unidentifiably complex mixture of aromatic molecules. The aforementioned crystals were cystallographically identified as 1,4,5,8-tetrachlorobiphenylene (Fig. S4.2B-D). **Space Group**: P 2_1/n (14), **Cell**: *a* 3.8455(5)Å *b* 14.531(3)Å *c* 9.8534(15)Å, *α* 90° *β* 92.535(13)° *γ* 90. [CCDC 2056845: Experimental Crystal Structure Determination: 1,4,5,8-tetrachlorobiphenylene]

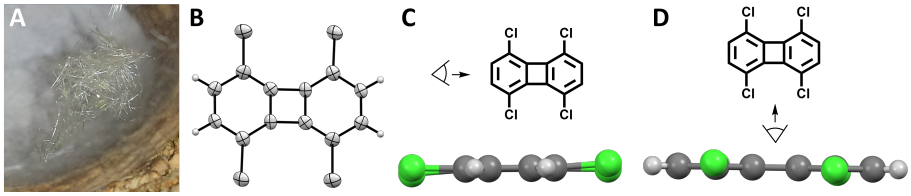

Figure S4.1 Crystals (A), ORTEP-styled drawing with ellipsoids at 50% probability (B), and two side views (C and D) of the crystal structure of 1,4,5,8-tetrachlorobiphenylene. Note that the aromatic structure is planar, whereas the chlorine atoms are bend out-of-plane in a "paired trans" fashion. Structures illustrated in B, C and D were generated with the Mercury 4.2.0 software suite.[43]

Computational. Equilibrium geometries of all structures were initially computed in the Spartan 10 program.[44] Computations were performed in the gas phase at the DFT level of theory using the ωB97X-D functional and 6-31G(d,p) basis set. The resulting structures were further refined using the Gaussian 09 Rev. D.01[45] program using the PBE functional[46] and 6-31G(d,p) basis set and using the D3(BJ) dispersion correction.[47,48] For structures containing I atoms the LANL2DZ (with effective core potential) basis set was used on I and a 6-31G(d,p) basis set on all other atoms.[49] Both the ωB97X-D and PBE functional are amongst the best performing in describing PAH structures.[50-53] Geometries were optimized in the gas-phase and subsequently re-optimized in combination with the SMD model to include solvent effects, using the appropriate solvent parameter.[54] The geometry convergence criteria were set to tight (Opt=tight; Max. Force = $1.5{\cdot}10^{-7}$, Max. Displacement = $6.0{\cdot}10^{-7}$), and an internally defined super-fine grid size was used (SCF=tight, Int= VeryFineGrid), which is a pruned 175,974 grid for first-row atoms and a 250,974 grid for all other atoms. These parameters were chosen because of the significant dependence of computed frequencies on the molecular orientation when using smaller grid sizes. This effect was particularly pronounced for transition metals and transition state structures.[55]

The denoted free Gibbs energy was calculated using Equation S1, in which ΔE_{gas} is the gas-phase energy (electronic energy), $\Delta G^{T}_{gas,QH}$ (T = 293.15 K, p = 1 atm., C = 1 M) is the sum of corrections from the electronic energy to the free Gibbs energy in the quasi-harmonic oscillator approximation, including zero-point-vibrational energy, and ΔG_{solv} is their corresponding free solvation Gibbs energy. The $\Delta G^{T}_{gas,QH}$ were computed using the quasi-harmonic approximation in the gas phase according to the work of Truhlar - the quasi-harmonic approximation is the same

as the harmonic oscillator approximation except that vibrational frequencies lower than 100 cm^{-1} were raised to 100 cm^{-1} as a way to correct for the breakdown of the harmonic oscillator model for the free energies of low-frequency vibrational modes.[56,57] All stationary points found were checked for either no imaginary frequencies for local minima or one imaginary frequency for transition state structures.

$$\Delta G^{T}_{solv} = \Delta E_{gas} + \Delta G^{T}_{gas,QH} + \Delta G_{solv} = \Delta G^{T}_{gas} + \Delta G_{solv} \quad \text{(Eq. S1)}$$

Transition states for the propellerene interconversion were obtained by first performing a dihedral angle scan in the Gaussian software to provide guess structures for a QST3 search. Transition states in the palladium(0) catalyzed reactions were obtained using a QST2 search. The obtained guess structures were optimized to a transition state using the Berny algorithm and confirmed by an intrinsic reaction coordinate calculation. The electronic energy fragments generated as described in the main text were computed at the same level of theory as the original propellerene molecules. Molecular structures were illustrated using CYLview.[58]

The activation strain model (ASM) analysis[24] and energy decomposition analysis (EDA)[33-35] were performed using the Amsterdam Density Functional (ADF2019.302)[59-61] software package based on the gas-phase structures obtained by Gaussian 09. The fragment-based approach was also performed using these optimized gas-phase geometries. Computations were performed using the PBE functional with D3(BJ) dispersion correction. The basis set used, denoted TZ2P, is of triple-ζ quality for all atoms and has been improved by two sets of polarization functions. The accuracies of the fit scheme (Zlm fit) and the integration grid (Becke grid) were, for all calculations, set to VERYGOOD. Relativistic effects were accounted for by using the zeroth-order regular approximation (ZORA). All computations were performed in the gas-phase.

Propellerene barrier heights to interconversion. To determine whether propellerenes are able to freely interconvert between their two conformations the barrier height for interconversion (*i.e.*, between the C_2 and D_3) was computed. This showed that for most the barrier heights are sufficiently height ($\Delta G^{\ddagger}_{C_2 \rightarrow D_3}$ > 24 kcal mol^{-1}) to prevent the spontaneous isomerization at room temperature (Table S4.1). On the other hand, for propellerene **1** the barrier height of interconversion is prohibitively low, so as to preclude isolation of the individual isomers ($\Delta G^{\ddagger}_{C_2 \rightarrow D_3}$ = 5.8 kcal mol^{-1}). Experimentally, the barrier heights for interconversion have been reported for a number of propellerenes and are in close agreement with computational results. Synthesis of propellerene **6** (tripyrenylene) was described in the previous Chapters. Variable temperature NMR experiments gave a barrier height to interconversion for **6** of 26.0 kcal mol^{-1}, which is in excellent agreement with the computed value of 25.8 kcal mol^{-1} (Fig. 3.2). For the unknown propellerene **7** computed values were compared to that of the known hexapole helicene from Kamikawa *et al.*, which were found to be in close agreement ($\Delta G^{\ddagger}_{C_2 \rightarrow D_3}$ = 7.6 *versus* 10.4 kcal mol^{-1}). Perfluorotriphenylene 1 was synthesized according to a known procedure,[12] and its ^{19}F NMR spectrum did not show any deconvolution or coalescence of the resonances at the technical limit of 173 K, indicating a barrier height below 8.8 kcal mol^{-1} (Fig. S4.2). Due to the unsuitability of perchlorotriphenylene **6** for variable temperature NMR experiments, hexachlorotriphenylene **14** was selected as model compound instead. Attempts to synthesize it were, however, unsuccessful (*vide supra*), yielding only the hitherto unknown 1,4,5,8-tetrachlorobiphenylene **15**, whose identity could be unequivocally stabilized from its crystal structure (See synthesis section above). Computed values for **6** were therefore compared to those reported for the known 4,5-dichloro-9,10-dihydrophenanthrene, which again shows close agreement ($\Delta G^{\ddagger}_{C_2 \rightarrow D_3}$ = 22.6 *versus* 24.2 kcal mol^{-1}).

Supplementary Figures and Tables

Table S4.1 Computed and experimental barrier heights for the conformer interconversion of benzoid and *ortho*-substituted propellerenes. All energies are reported with respect to the $C_2 \rightarrow D_3$ transition, and are expressed in kcal mol^{-1}. Computed at the SMD-PBE-D3(BJ)/6-31G(d,p) level of theory. Solvent parameter corresponds with experimental conditions.

	Preference (exp.)	$\Delta\Delta G_{solv.}$ (comp.)	$\Delta G^{\ddagger}_{C_2 \leftrightarrow D_3}$ (exp.)	$\Delta G^{\ddagger}_{C_2 \leftrightarrow D_3}$ (comp.)
1	C_2	4.2	<8.8	5.8
2	C_2	4.0	22.6[62,63]	28.8
3	C_2	2.9	---	34.9
4	C_2	4.5	>28.0[9,64]	31.0
5	D_3	–3.6	26.2[22]	25.1
6	D_3	–3.4	26.0	25.8
7	D_3	–3.0	---[19]	23.3
8	D_3	–3.4	---	28.7

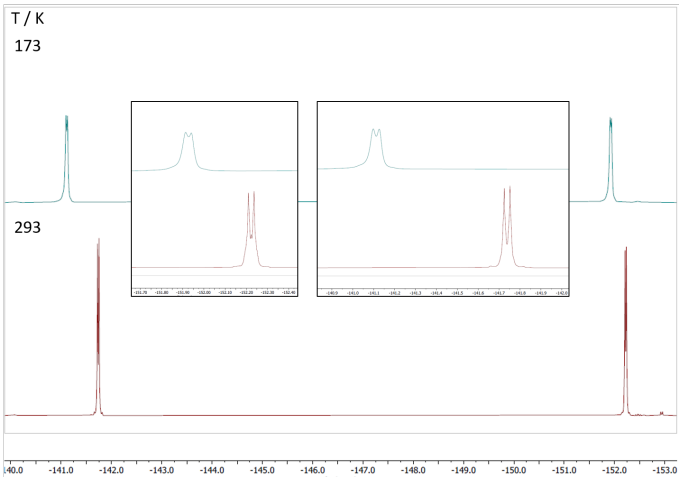

Figure S4.2 ^{19}F VT-NMR spectra of perfluorotriphenylene **1** in THF-d_8.

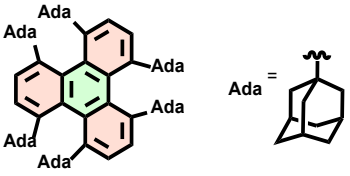

12

Figure S4.4 Structure of compound **12**.